

# Crack propagation and fracture toughness of solid balsa used for cores of sandwich composites

Meisam Shir Mohammadi and John A Nairn

Wood Science & Engineering, Oregon State University, USA

## Abstract

To better understand the suitability of balsa wood as a core material for sandwich composites, this paper presents a detailed study of the fracture properties of balsa. The experiments looked at mode I, mode II, and mixed-mode fracture with crack growth both parallel and perpendicular to the wood grain direction. The experiments monitored toughness as a function of crack growth to record crack resistance or  $R$  curves. The mode I toughness was lower than most other wood species, but considering its low density, the toughness of balsa is higher than previously expected. The mode I toughness increased as a function of crack growth due to a fiber bridging process zone at the crack tip. The mode II toughness was higher than mode I toughness, but was much less affected by fiber bridging. The mixed-mode failure envelope had an unusual shape, which could be explained by an influence of fiber bridging. Overall, the toughness of balsa is adequate for sandwich composite core materials and likely better than some alternative core materials.

## Keywords

Balsa, fracture, fiber bridging, core material,  $R$  curve

## Introduction

Balsa wood is an interesting natural material with one important application being as a core material in sandwich composite structures. Balsa is mostly found in tropical areas such as Ecuador in South America. The word *balsa* is Spanish for *raft* and has its historical roots among Polynesian people. Around 500 A.D Peruvians used balsa trees to construct their Kon-Tiki rafts.

---

### Corresponding author:

John A Nairn, Wood Science & Engineering, Oregon State University, Corvallis, OR 97330, USA

Email: John.Nairn@oregonstate.edu

Being the softest and the lightest commercial wood, balsa's density is low and varies over a wide range (from 0.04 to 0.32 g/cm<sup>3</sup>) that depends on age and tree habitat (Easterling *et al.*, 1982). In the United States, balsa was used in aircraft in the 1920s. It has also been used for construction of gliders and as part of the body of the World War II Mosquito fighter plane (Easterling *et al.*, 1982).

Balsa is a common core material for sandwich composites used in boats, wind turbine blades, bridge decks, *etc.* (Easterling *et al.*, 1982). Balsa sandwich composites have the same advantages as other sandwich composites (*e.g.* foams and honeycomb cores), namely ultra low weight and considerable stiffness, making it a competitive alternative core material (Strong, 2008). At the same time, they share the general concerns of local crushing or bruising of the core material, or some other material-specific failure mechanism (Strong, 2008). For these reasons, it is important to study the deformation and failure properties of balsa wood. A number of studies have investigated its mechanical properties, but few have specifically addressed fracture toughness. Easterling *et al.* (1982) generated and analyzed compressive stress-strain curves for medium density balsa wood. Dreisbach (1952) reported a numerical value for fracture toughness, but did not address the method used for the measurement. Given the history of experimental measurements for the toughness of wood (see below), the results from Dreisbach (1952) may not be reliable. Ashby *et al.* (1985) measured fracture toughness of balsa, but looked only at initiation, did not distinguish crack planes for cracks parallel to the fibers, and used lower density balsa than now commonly used in structural sandwich composites. Gibson and Ashby (1997) considered the fracture toughness of various woods as a function of density and suggested they following scaling law:

$$K_{Ic} = D \left( \frac{\rho}{\rho_c} \right)^2 \quad (1)$$

where  $K_{Ic}$  is fracture toughness (as critical stress intensity factor),  $\rho$  is the density of wood,  $\rho_c$  is the density of cell wall material, and  $D$  is a constant. An alternate measure of toughness is critical energy release rate  $G_{Ic}$  or energy per unit growth of fracture area. Because  $G_{Ic}$  is related to square of  $K_{Ic}$  (Atkins and Mai, 1985), equation (1) predicts that  $G_{Ic}$  scales with density to the fourth power. Because density of balsa is often two or more times lower than other wood, this scaling law, if held to be applicable, predicts very low toughness for balsa and suggests it may

have inferior properties to serve as a robust core material. The purpose of this work was to use modern methods for characterizing fracture properties of wood to derive a more complete study of the fracture properties of balsa wood.

Early work on wood fracture measured the toughness of wood by classical fracture mechanics methods (e.g., Atack et al., 1961; DeBaise *et al.*, 1966; Schniewind *et al.*, 1971, 1973; Johnson, 1973; Jeronimidis, 1980). The typical experiments are to prepare standard fracture mechanics specimens, such as single-edge notched specimens in bending or tension or compact tension specimens, load them to initiation of failure, and then calculate toughness as a stress intensity factor using standard calibration functions (Williams, 1984). But using this approach for wood fracture may not be appropriate. Wood, like many composite materials, can have a complex cracking process zone left in the wake of a propagating crack tip. In wood, the wake can have fibers that bridge across the crack plane and continue to carry load. Because classical fracture mechanics methods assume a stress-free fracture surface, any fracture parameters calculated by those methods will not give the most accurate toughness for the material. Furthermore, because of the fiber-bridging zone, the toughness will change as the crack propagates (Atkins and Mai, 1985). Thus standard experiments that measure initiation only are, at best incomplete and, at worst, have invalid results.

A more complete characterization of the fracture properties of wood requires two changes. First, the experiments must monitor toughness as a function of crack growth. For materials with fiber bridging effects, the toughness will increase with crack growth and a plot of toughness vs. crack growth is the material's *R* curve. Full characterization of wood requires experiments to measure *R* curves. Second, because the fiber-bridging zone complicates analysis of crack-tip stress states, common methods for evaluating toughness should not be used. One alternative is to directly measure energy released by crack growth from force-displacement-crack length experiments during crack growth. This approach avoids any need to make assumptions about stress-free fracture surfaces and therefore accounts for fiber bridging or friction, if they occur. It has been applied to several species of wood before (Matsumoto and Nairn, 2009, 2012; Wilson *et al.*, 2013). Here these direct energy methods were used to characterize fracture properties of balsa wood.

Besides the need to measure full *R* curves for balsa wood, balsa is an anisotropic material. The trunk of a tree is approximately cylindrically orthotropic. When cut into small, rectangular

specimens, each one will be approximately planar orthotropic with three planes of symmetry having normal vectors in the radial (R), tangential (T), and longitudinal (L) directions of the original tree. Within each plane, crack propagation may be in the two other orthogonal directions. The standard fracture propagation nomenclature for these six crack-growth directions are defined by two letters, namely, RL, RT, TL, TR, LT, and LR (Schniewind and Centeno, 1971; Johnson, 1973). The first letter is the direction of the normal vector for the crack plane while the second letter is the direction of crack propagation. Full characterization of wood fracture requires experiments in all crack paths, although LT or LR cracks cannot be studied for crack propagation because such cracks always turn to become RL or TL cracks, rather than propagate as LT or LR cracks. This work measured opening mode (mode I) toughness for all remaining directions — for RL, TL, RT, and TR. Additional experiments measured shear mode (mode II) toughness for RL and TL directions. In a few of the mode I specimens, the crack deviated from the mode I direction due to grain orientation in those specimens. This deviation caused mixed-mode loading. These specimens could therefore be used to get some information of mixed-mode failure of balsa wood. Overall the toughness of balsa wood is lower than other species, but can increase with crack growth due to fiber bridging. Considering its very low density, however, its toughness is higher than was expected by prior scaling predictions derived from cellular mechanics (Gibson and Ashby, 1997).

## **Materials and methods**

The balsa wood used in this work was supplied by 3A Composites. All samples were stored in a conditioning room (20°C and 65RH) prior to testing resulting in equilibrium moisture content of about 12%. The densities at 12% moisture content ranged from 0.15 to 0.35 g/cm<sup>3</sup>. To assess the role of density on fracture, we recorded the density of each specimen from a region along the crack path by cutting out a block of wood and measuring its weight and dimensions. The mode I fracture energy for RL, TL, RL45, RT, and TR directions were measured using double cantilever beam (DCB) specimens. Here RL, TL, RT, and TR are as defined in the introduction. The RL45 specimens were specimens where the growth rings were at 45° to the ends of the specimen. Therefore, when a notch was cut in the DCB specimen, the normal to the crack plane was also at 45° to the R direction. The crack still propagated in the L direction. For

the three longitudinal directions (RL, TL, and RL45), the length, width and thickness of the specimens were 200, 25 and 25 mm, respectively, with an initial crack length of 75 mm (see Figure 1). For the two perpendicular directions (RT and TR), the specimen length was limited to 140 mm due to diameter of the balsa trees and extent of available material cut in the diameter direction. We tried glued up material (provided in block form), but the glue joints failed. Instead the perpendicular direction experiments were done on smaller specimens with length, width and thickness of 135, 40 and 36, respectively, and initial crack length of 35 mm. A total of five specimens were tested for each direction, some of which were used to study the effects of sharp crack tip created using razor blades. The displacement rate was 2 mm/min using an Instron 5582 testing frame. During testing, we recorded load and displacement. The displacement near the load point was measured with an LVDT mounted on the specimen. To observe crack lengths, an automated camera system took periodic pictures synchronized with time stamps corresponding to the force and displacement data. All data were collected under ambient conditions soon after removing specimens from the conditioning room.

Mode II experiments were done only in the RL and TL directions using the four-point end-notched flexure (ENF4) specimen illustrated in Figure 1. These specimens were loaded at four points with the initial crack under one of the central load points. The first specimens failed by indentation of the balsa at the load points due to the high loads needed to propagate the crack. By simple beam analysis, the mode II energy release rate is proportional to moment squared where the moment is load-point force ( $P/2$  at each load point)  $\times$  distance between the outside supports ( $d$ ) (Martin and Davidson, 1999):

$$G_{II} = \frac{9P^2 d^2}{2EB^2 h^3} \quad (2)$$

To reduce the load ( $P$ ) needed to reach critical  $G_{II}$  for crack growth, we used long specimens (length = 500 mm) and increased the distance between the outside supports ( $d$ ) to 200 mm. To further limit indentation at support-points, plateau supports were used to distribute the force. The flexural rate was 3 mm/min using an Instron 5582 testing frame. The specimen cross section was 25  $\times$  25 mm. With this geometry, we got crack propagation without damaging the loading points. Although  $G_{II}$  in equation (1) is independent of crack length, Martin and Davidson (1999) have shown by simple beam theory that  $dG_{II}/da < 0$  at constant displacement, which suggests crack growth should be stable (Williams 1984). This simple beam theory ignores friction and fiber

bridging. For materials with a rising  $R$  curve, stable crack growth only requires  $dG_{II}/da < dR/da$  (at constant displacement) (Williams 1984). In short, the ENF4 specimen is recommended for stable pure mode II crack growth and we did get stable crack growth in ENF4 balsa specimens.

The key challenge for fracture experiments with solid wood (as well as both wood and non-wood composites) is accurately determining the crack length. In mode I experiments, crack lengths could be measured by careful observation of the synchronized images. In mode II experiments, however, the crack surfaces do not open, which makes visual crack length observation unreliable. We instead used digital image correlation methods (DIC) to optically record displacement fields from which we could determine shear strain (Sutton, 1983). Figure 2 shows a series of measured shear strains as a function of distance from the initial crack tip along a line ahead of the crack tip. The different plots are at different times during the experiment. Clearly the shear strain is high near the crack tip and decreases with distance from the crack tip. Although it was not possible to locate the exact crack tip in DIC results, the energy analysis method described below only needs crack growth or  $\Delta a$ . We found  $\Delta a$  by the distance between two curves at the location where the shear strain was 1% (see Figure 2; this strain value was altered slightly depending on specimen). Adding up a sequence of  $\Delta a$ 's gave total crack length for use in the analysis described below. The results for  $\Delta a$  were insensitive to the specific shear strain chosen (*e.g.*, within the 0.5% to 1.5% range), because the shear strain plots maintained a similar shape and only shifted due to crack growth.

Analysis of wood fracture data requires observation of changes in toughness as a function of crack length known as the  $R$  curve. We used the method described in Nairn (2009), Matsumoto and Nairn (2012) and Wilson *et al.* (2013), which is illustrated in Figure 3. Figure 3(left) shows force and crack length as a function of displacement. Using custom Java software, the data reduction calculated the cumulative energy released, as illustrated by the shaded area in Figure 3(left), as a function of displacement (the right edge of the shaded region). This energy was cross-plotted as a function of crack length at the corresponding displacement as shown in Figure 3(right). The slope of this curve divided by specimen width is the energy release rate toughness as a function of crack length or a direct calculation of the  $R$  curve. The slope was calculated by linear fit to a portion of the data using a sliding window (of user-adjustable size) along the curve to get slope as a function of crack length. Because  $R$  depends only on slope, the absolute crack length is not needed; but experiments always need accurate results for  $\Delta a$ . Some typical  $R$  curves

are given in Figure 4 and they generally increased with crack length due to development of a fiber-bridging process zone. An increasing  $R$  is visible in a total energy plot (such as in Figure 3(right)) as a positive curvature. The energy calculated by the shaded area assumes unloading would be elastic and return to the origin. Experimental observations show this assumption is reasonable for wood (Matsumoto and Nairn, 2009). The reason unloading should be avoiding is because bridging fibers might interfere with unloading (Atkins and Mai 1985), which means the unloading process could damage those fibers thereby changing the toughness for subsequent crack propagation. After each test, specimen densities for regions near the crack tip were measured to investigate the effect of density on  $R$  curves.

## Results

### *Mode I parallel to the grain - RL, TL, and RL45*

RL, TL, and RL45 fracture all have cracks running parallel to the wood fiber direction but propagate in different fracture planes. Figure 4 plots the collected  $R$  curves for five individual specimens in the RL direction. The plots give  $R$  curve as a function of crack growth by subtracting initial crack length of each specimen (about 75 mm) from measured total crack length. Occasionally, a specimen had unstable crack growth. Although non-steady crack growth can be analyzed (Wilson *et al.* 2013), the method used here for a continuous  $R$  curve works best with stable and steady crack growth. Specimens with regions of unstable crack growth were attributed to local defects and not included in these analyses.

RL specimen with density  $0.22 \text{ g/cm}^3$  (#1) used an unmodified band-sawn kerf (blade thickness of 0.5 mm) for its initial notch; the toughness started at around  $45 \text{ J/m}^2$  and increased to over  $60 \text{ J/m}^2$  after about 30 mm of crack growth and then remained fairly level. To test initial crack preparation methods, RL specimen with density  $0.19 \text{ g/cm}^3$  used a razor blade to sharpen the initial band-sawn kerf. It started at about the same toughness of  $50 \text{ J/m}^2$ , increased to about  $60 \text{ J/m}^2$  at about 30 mm of crack growth and then continued increasing, eventually exceeding  $140 \text{ J/m}^2$ . The start of the  $R$  curves for these two samples were very similar indicating that initial crack preparation had little affect on wood fracture testing. Unlike homogeneous materials where initial crack preparation can influence crack initiation (Crouch *et al.*, 1992), the complexities of wood anatomy and dimensions of wood cells (50 to 100  $\mu\text{m}$ ) apparently result in experiments on

band-sawed vs. razor notched specimens that have no consistent differences. The  $R$  curves for these two specimens differ after 30 mm of crack growth, but that difference is certainly unrelated to initial notch preparation. Instead, the large increase in the  $\rho = 0.19 \text{ g/cm}^3$  specimen after 30 mm of crack growth corresponded to an observed deviation of the crack plane from the specimen midplane as shown in Figure 5. In other words, when a mode I  $R$  value increases in a wood DCB specimen, the increase could be caused by a fiber bridging zone, by mixed mode behavior due to sample asymmetry when a crack deviates from midplane, or by a combination of these two effects. Comparing RL samples  $\rho = 0.22 \text{ g/cm}^3$  (#1) and  $\rho = 0.19 \text{ g/cm}^3$ , we concluded that the rise in the former was due to fiber bridging (because the crack in that specimen remained straight) while the rise for the later, which deviated, additionally had mixed mode effects. The contribution of mixed mode loading is analyzed further below.

Additional RL samples  $\rho = 0.22 \text{ g/cm}^3$  (#2),  $\rho = 0.26 \text{ g/cm}^3$ , and  $\rho = 0.34 \text{ g/cm}^3$  illustrate variability in balsa fracture toughness and possible effects of density. RL sample  $\rho = 0.22 \text{ g/cm}^3$  (#2) had a nearly constant  $R$  curve at about  $75 \text{ J/m}^2$  and it had a low density. RL sample  $\rho = 0.26 \text{ g/cm}^3$  had a slightly higher density and a slightly higher toughness and rising  $R$  curve from  $80 \text{ J/m}^2$  to  $100 \text{ J/m}^2$ . For RL sample  $\rho = 0.34 \text{ g/cm}^3$ , the  $R$  curve started from  $75 \text{ J/m}^2$  and increased up to  $125 \text{ J/m}^2$  after 50 mm of crack growth. This specimen had the highest toughness and also had the highest density.

The dashed curve shows an average RL toughness for all curves except the  $\rho = 0.19 \text{ g/cm}^3$  specimen, which was eliminated because of its crack deviation. This averaging combined specimens with band-sawn and razor-sharpened notches because we did not notice any significant effects of notch preparation on  $R$  curves. The average was found by averaging within 10 windows along the data. The error bars are standard deviations of all points within each window. The trend that emerges in RL fracture is a toughness that starts in the range of 50 to  $60 \text{ J/m}^2$  and increases by  $30 \text{ J/m}^2$ , most likely due to fiber bridging. It is possible the toughness increase has stopped after about 50 mm of crack growth, indicating a steady-state RL toughness of about  $90 \text{ J/m}^2$ . The role of fiber bridging was confirmed by observation of fibers bridging the crack by optical microscopy, but the increase was smaller than observed in other species (e.g., Douglas fir, pine, (Wilson *et al.*, 2013)) indicating a smaller contribution of fiber bridging in balsa than in other species. If the crack deviates, as in RL sample  $\rho = 0.19 \text{ g/cm}^3$ , the toughness can increase faster, most likely due to contribution of mode II loading. Although this averaging

included samples with different densities, we claim it presents an expected  $R$  curve for balsa RL fracture. In other words, we observed specimen-to-specimen variations with similar densities that were often larger than variations between specimens with different densities.

Figure 6 plots three  $R$  curves for TL fracture. Again, no significant differences were seen between band-sawn and razor-sharpened cracks and therefore all results are discussed together. In TL specimen with  $\rho = 0.23 \text{ g/cm}^3$ , the crack remained straight during propagation. The  $R$  curve started at about  $140 \text{ J/m}^2$  and increased to  $150 \text{ J/m}^2$  after 80 mm of crack growth. The slight increase again indicates fiber bridging (as observed in Figure 7), but the small increase indicates a smaller role for bridging in balsa than in other species (Wilson *et al.*, 2013). Furthermore, while other species show a larger role for fiber bridging in TL fracture than in RL fracture (Wilson *et al.*, 2013), the toughness increase was similar for RL and TL direction in balsa. The  $R$  curve for TL specimen with  $\rho = 0.27 \text{ g/cm}^3$  started at  $135 \text{ J/m}^2$  and increased to  $150 \text{ J/m}^2$  and then was close to constant. TL specimen with  $\rho = 0.32 \text{ g/cm}^3$  had the highest density and a slightly higher  $R$  curve. Its  $R$  curve started at  $130 \text{ J/m}^2$  and increased to  $200 \text{ J/m}^2$ . After about 50 mm of crack the toughness of  $\rho = 0.32 \text{ g/cm}^3$  specimen was higher than the other two, but this position also corresponded to some deviation of the crack from the midplane, as shown in Fig 7. The higher toughness in the  $\rho = 0.32 \text{ g/cm}^3$  specimen could be due to mixed mode effects, which will be discussed below.

The dashed curve in Figure 6 plots the average TL  $R$  curve, but omits the specimen with  $\rho = 0.32 \text{ g/cm}^3$  because of its crack deviation. The overall toughness for TL fracture was more than twice the RL toughness (Figure 6 re-plots the average RL  $R$  curve, without error bars, for comparison). Comparing Figs. 4 and 6, the specimen-to-specimen variations were slightly larger for RL fracture than for TL fracture and the effect of density might be slightly larger for RL fracture as well. The difference between TL and RL fracture planes is that TL fracture planes cross multiple growth rings while RL planes can remain confined to one low-density growth ring region. The observed differences suggest that TL fracture is higher due to forced contribution of more higher-density regions. Note that we could only record bulk density and not account for local density along the crack path. The density effect on RL fracture should depend on the local low-density region for crack growth, while the TL fracture will depend more on an average of the spanned higher density regions. It is difficult to sort out these dependencies when only global specimen densities are known.

Cracks propagating parallel to the wood fibers may potentially make any angle with growth rings. To test the effect of that angle, specimens were selected with growth rings at about  $45^\circ$  to the crack plane for specimens denoted here as RL45 fracture, or crack surface normal rotated  $45^\circ$  from the radial direction. The RL45 samples had more variable results and perhaps were affected by initial notch preparation. Two specimens with  $\rho = 0.17 \text{ g/cm}^3$  and  $\rho = 0.27 \text{ g/cm}^3$  had band-sawn initial crack tips. In each sample, the crack grew unstably after initiation for about 20 mm and thereafter was stable. The resulting  $R$  curves in Figure 8, which missed information about initial toughness, were at about  $100 \text{ J/m}^2$  and mostly flat (*i.e.*, no evidence of additional fiber bridging) or dropped. These two samples had different densities, which suggests that like TL fracture, density does not have much effect on RL45 fracture. Two RL45 samples with  $\rho = 0.28 \text{ g/cm}^3$  and  $\rho = 0.30 \text{ g/cm}^3$  were cut from a different block with higher density and had razor-sharpened initial crack tips. Both samples started with stable crack growth. The  $\rho = 0.28 \text{ g/cm}^3$  curve started at about  $160 \text{ J/m}^2$  and increased monotonically to  $205 \text{ J/m}^2$ . The crack path remained straight and the images had visual evidence of fiber bridging. The  $\rho = 0.30 \text{ g/cm}^3$  curve also started from  $160 \text{ J/m}^2$ , but was more erratic and turned to higher values and higher slope after 22 mm. This point corresponded to the point at which the crack in this specimen turned and deviated from the mid plane and become unstable.

Although there was more variability in RL45 fracture, we averaged the three samples with straight cracks (RL45 specimens with  $\rho = 0.17, 0.27,$  and  $0.28 \text{ g/cm}^3$ ). The average is plotted in Figure 8 and included only crack growth regions seen by all specimens. This RL45 toughness was similar to the TL fracture  $R$  curve (re-plotted in Figure 8 without error bars) suggesting that high toughness is controlled by the crack front crossing a sufficient number of growth rings. Both average TL and RL45  $R$  curves were significantly higher than the RL fracture  $R$  curve.

### *Mode I perpendicular to the grain - RT and TR*

An RT crack grows in the same fracture plane as an RL crack, but the crack direction is perpendicular to the wood grain direction rather than parallel. Similarly, TR fracture is in the same plane as a TL crack but growing perpendicular to the fibers. Because the crack planes are the same, the RT and TR toughnesses might be expected to be similar to TL and RL, but there are also differences, which make RT and TR experiments worthwhile. Unlike RL, TL, and 45RL fracture where propagation is controlled by wood grain direction, including deviations from the

midplane when the grain angle is tilted, RT and TR cracks can potentially turn and propagate in any direction. There are no wood fibers to block them. As a result, the crack growth is inherently less controlled. If a specimen has curved growth rings or regions of lower toughness, the crack may turn making it difficult to monitor toughness during crack growth. Indeed, we were only able to achieve sufficiently straight crack growth to get  $R$  curve results for RT fracture. When TR specimens were loaded, the cracks turned to become RT cracks. We can conclude that TR toughness is higher than RT toughness, but could not measure  $R$  curves for TR crack growth. One might expect radial ray cells (*i.e.*, wood cells in the radial direction associated with moisture transport (Haygreen and Bowyer, 1995)) to block RT crack growth and promote TR crack growth, but apparently rays cells in balsa wood provide little or no resistance to the tangential crack growth direction of RT cracks.

Even in the RT direction, it was difficult to maintain straight propagation, but by using wider specimens (36-40 mm) we were able to get stable crack growth and measure  $R$  curves for five specimens, which are plotted in Figure 9. The  $R$  curves started from different values from as low as  $90 \text{ J/m}^2$  to as high as  $380 \text{ J/m}^2$ . All  $R$  curves increased monotonically with similar slopes indicating the development of a fiber bridging or a fracture process zone. The RT toughness was more affected by density. For example the RT sample with highest density ( $\rho = 0.275 \text{ g/cm}^3$ ) had the highest mode I high toughness of any specimen; it started at  $380 \text{ J/m}^2$  and increased to about  $500 \text{ J/m}^2$ . Because of this density effect and the large variability, we did not calculate an average  $R$  curve for RT fracture. In general, the RT toughness was higher than RL toughness, which is crack growth in the same plane but in the L direction instead of the T direction. It was similar to or higher than TL and RL45 toughness. The RT toughness also increased faster with crack length. Notice that the total amount of RT crack growth was smaller, thus the observed increase happened much faster than in RL, TL, or RL45 fracture.

### *Mode II parallel to the grain*

$R$  curves are not commonly measured in mode II because it is difficult to achieve stable crack growth and difficult to observe crack length. The latter difficulty is because unlike mode I cracks, mode II cracks do not open and visualization alone is inadequate for measuring crack lengths. We solved the stability problem by using the ENF4 specimen, which is theoretically stable when loaded in displacement control (Martin and Davidson, 1999). Furthermore,

specimens that have process zones can have enhanced stability if  $R$  increases with crack growth (Williams, 1984). We solved the crack observation problem by using DIC methods as discussed above (Sutton *et al.*, 1983). To emphasize, all crack lengths in mode II were measured using DIC methods because it was not possible to optically detect the crack growth needed for accurate  $R$  curve analysis.

Figure 10 shows the  $R$  curves for three mode II specimens in the RL direction. Overall, we judged the curves as approximately flat. In other words, even if fibers bridge the mode II crack, they do not carry enough load to influence the  $R$  curve. The averaged curve is characterized as roughly constant and equal to 250-350 J/m<sup>2</sup>. The initial toughness was a little higher, but it depended on just one specimen. Since  $R$  curves with process zones normally do not drop, the drop in this averaged curve is more likely a consequence of specimen-to-specimen variations. The  $R$  curve was flattest in regions that averaged all three specimens.

Figure 11 shows three mode II specimens in the TL direction. The results were similar to RL fracture, although one specimen ( $\rho = 0.2 \text{ g/cm}^3$ ) showed rather large oscillations. Such oscillations could be due to either a real variation in toughness along the crack path, or to the difficulty in measuring crack length in mode II. If the actual crack growth was underestimated in one region and then compensated by overestimation in another region, it could lead to such an oscillation. In contrast a change local toughness would change values, but would not, except by chance, result in oscillations. For these reasons, it is more likely that the mode II toughness is roughly constant. The averaged  $R$  curve shows TL toughness of about 250-350 J/m<sup>2</sup> and to be roughly constant and similar to the RL curve (which is included for comparison without error bars). In summary, RL and TL mode II toughnesses are similar, roughly constant, little affected by fiber bridging, and higher than mode I toughness.

## Discussion

These experiments provide a fairly complete picture of the fracture properties of balsa. We measured mode I fracture in four directions — RL, TL, RL45, and RT. The TR direction could not be measured because the cracks always turned to become RT cracks. Similarly, LR and LT cracks are not relevant because cracks will not propagate in the L direction through wood fibers, but will turn to become RL or TL cracks. We also measured mode II toughness in two directions

— RL and TL. Unlike previous studies, which looked only at initiation (Easterling *et al.*, 1982), all these experiments looked at both initiation and propagation of cracks. The main findings are that all mode I results showed increasing  $R$  curves indicating a contribution of fiber bridging to toughness. TL and RL45 toughnesses were higher than RL toughness. The highest toughness was in the RT direction with a high-density specimen. The mode II toughness was higher than the mode I toughness and much less affected (or unaffected) by fiber bridging.

Although toughness of wood has often been measured, few studies have looked at full  $R$  curves during crack propagation. One exception is Conrad *et al.* (2003), although their beam analysis methods do not explicitly account for fiber bridging. Another exception is a recent paper from our group (Wilson *et al.*, 2013) that used the same methods used in this paper for five other species of wood - cedar, Douglas fir, hemlock, pine and oak. Compared to these species, the  $R$  curves for balsa were comparable to cedar, but lower than other species. Like balsa, cedar is a low-density wood. The differences between balsa and other species however were not large. Douglas fir, hemlock, and pine (RL direction) had  $R$  curves starting about 100-160 J/m<sup>2</sup> that increased to 200-300 J/m<sup>2</sup> after crack growth. Only oak and pine (TL direction) had much higher toughnesses starting at 300 J/m<sup>2</sup> and increasing to 600 J/m<sup>2</sup>. Comparing the magnitudes of the increase in  $R$  with crack growth, the low-density species (balsa here and cedar in Wilson *et al.* (2013)) showed a much smaller increase than higher density species. Thus fiber bridging plays a smaller role in toughness for low-density wood.

Ashby *et al.* (1985) measured  $K_{Ic}$  for initiation of cracks parallel to fibers and found it to range from 0.025 to 0.14 MPa  $\sqrt{m}$  for specimens with densities ranging from 0.05 to 0.15 g/cm<sup>3</sup>. They looked only at initiation and did not distinguish between RL and TL fracture. Our initial values of 60 J/m<sup>2</sup> for RL fracture and 130 J/m<sup>2</sup> for TL fracture can be converted to  $K_{Ic}$  by using orthotropic conversions (Kanninen and Popelar 1985) applied to RL and TL fracture (Matsumoto and Nairn 2012) along with longitudinal modulus of balsa (our specimens averaged  $E_L = 4320$  MPa) and typical modulus ratios and Poisson ratios for balsa in the Wood Handbook (Forest Products Laboratory 2010). After the conversions, we measured  $K_{Ic} = 0.28$  MPa  $\sqrt{m}$  for both RL and TL crack initiation. These results are higher than Ashby *et al.* (1985), possibly because our specimen densities were higher (ranging from 0.19 to 0.34 g/cm<sup>3</sup>).

Density affects many wood properties and it plays a role in toughness. One qualitative analysis by Gibson and Ashby (1997) using cellular mechanics predicts that toughness (as an

energy release rate) in low-density wood should scale as density to the fourth power (see square of equation (1)). By this scaling and the results in Wilson *et al.* (2013) for Douglas fir, hemlock and pine, which all have density of about 0.45 and  $R$  curves that initiate at about  $130 \text{ J/m}^2$  and increase to about  $250 \text{ J/m}^2$ , the expected toughness for balsa wood with density around 0.22 should be 16 times lower or initiate at  $8 \text{ J/m}^2$  and increase to only  $16 \text{ J/m}^2$ . But experimental results are much higher than this prediction. In other words, the cellular mechanics models for toughness overestimates the role of density. As a consequence, the use of balsa in applications that need low density, such as sandwich composites, can be done without sacrificing too much toughness. In these applications, balsa is often a replacement for polymeric foams (which can be extremely brittle (Gibson and Ashby, 1997)) and likely has sufficient or even enhanced toughness properties.

These experiments focused on mode I and mode II  $R$  curves for balsa along various crack paths. A more complete fracture characterization should include mixed-mode crack growth as well. Mixed-mode toughness is commonly characterized by plotting  $G_{II}$  vs.  $G_I$  at failure from a series of specimens having different  $G_{II}/G_I$  ratios. These results will be equal to mode I toughness ( $G_{Ic}$ ) when  $G_{II} = 0$  and equal to mode II toughness ( $G_{IIc}$ ) when  $G_I = 0$ . The curve shape between these two points describes the mixed-mode failure envelope for the material. A few of our mode I specimens (such as RL  $\rho = 0.19 \text{ g/cm}^3$ , TL  $\rho = 0.32 \text{ g/cm}^3$ , and RL45  $\rho = 0.30 \text{ g/cm}^3$  specimen) did have crack growth that followed tilted grain angle and therefore deviated from the midplane. Such deviations seemed to correspond with larger increases in  $R$  curve than in specimens that did not deviate from the midplane. When a crack in a DCB specimen deviates from the midplane, however, the specimen becomes an asymmetric because of an off-center crack. The consequence of an off-center crack is that the loading is no longer pure mode I, but rather becomes mixed mode (Williams, 1988). The amount of mode II depends on location of the crack tip. We made use of specimens with deviations to determine a portion of the mixed-mode failure envelope for balsa and to assess the role of fiber bridging on such envelopes.

The specimen with the most deviation was the RL  $\rho = 0.19 \text{ g/cm}^3$  specimen (see Figure 5) and it therefore provided the largest amount of mode mixity for evaluating a failure envelope. The first task was to determine the  $G_{II}/G_I$  ratio as a function of crack deviation. This task was done using finite element analysis (FEA) with crack closure methods (*e.g.*, Nairn, 2011) to determine total energy release rate,  $G$ , and mode I component,  $\varphi = G_I / G$ , as a function of the

ratio  $h_2/(h_1+h_2)$  in DCB specimens. Here,  $h_1$  is the distance from the crack tip to the farther surface and  $h_2$  is the distance to the closer surface (see Figure 1). The FEA results are in Table 1. To achieve convergence, the calculations were done for a regular mesh of equal size elements, those element sizes were varied, and finally the results were extrapolated to zero element size (Nairn, 2011). The total  $G$  converged very rapidly, but accurate mode I component required this extrapolation method. Next, a mixed mode failure envelope was calculated from experimental results as follows:

1. Find  $R$  at a specific amount of crack growth.
2. Look at the image corresponding to that crack length, measure  $h_1$  and  $h_2$ , calculate  $h_2/(h_1+h_2)$ , and interpolate  $\phi$  from FEA results in Table 1.
3. Find  $G_I = \phi * R$  and  $G_{II} = R - G_I = (1-\phi) * R$
4. Plot mixed-mode failure diagram for  $G_{II}$  as a function of  $G_I$  at failure and optionally include  $G_{IIc}$  point from mode II tests (*i.e.*, plotted at  $G_I = 0$ ).

Figure 12 shows mixed-mode envelope for RL  $\rho = 0.19 \text{ g/cm}^3$  specimen. Curiously, the  $G_{II}$  component increased as the  $G_I$  component increased. A common, empirical relation between  $G_{II}$  and  $G_I$  during mixed-mode loading is a failure envelope defined by

$$\left(\frac{G_I}{G_{Ic}}\right)^a + \left(\frac{G_{II}}{G_{IIc}}\right)^b = 1 \quad (3)$$

where  $G_{Ic}$  and  $G_{IIc}$  are the pure mode I and mode II toughnesses and  $a$  and  $b$  are exponents. For example if  $a = b = 2$  (a common approximation), the  $G_{II}$  vs.  $G_I$  curve is one quadrant of an ellipse. This relation predicts a convex monotonic surface such that  $G_I$  always drops as  $G_{II}$  increases. This shape does not agree with our results that showed both  $G_I$  and  $G_{II}$  increasing as the crack deviates.

The problem in materials with  $R$  curves is that there is no single  $G_{Ic}$  or  $G_{IIc}$  to use in equation (3), but rather an  $R$  curve with variable toughness at each mixed-mode ratio. For balsa, we observed flat  $R$  curves for mode II and thus  $G_{IIc}$  is approximately constant, but  $G_{Ic}$  (or  $R$ ) increased as the crack propagated. For such a material the mixed-mode description needs a 3D surface with crack growth on the third axis. This 3D surface can be represented by a family of  $G_{II}$  vs.  $G_I$  failure envelopes with each curve being for constant amount of crack growth or for a

fixed extent of fiber bridging. Figure 13 illustrates this hypothesis. Curve 1 is a mixed-mode envelope with  $a = b = 2$ ,  $G_{Ic} = 95 \text{ J/m}^2$  and  $G_{IIc} = 250 \text{ J/m}^2$ . Curves 2 and 3 show new envelopes at different amounts of crack growth where  $G_{Ic}$  has increased to 110 or 125  $\text{J/m}^2$  but  $G_{IIc}$  has remained constant. In real experiments the crack is always growing, which means the measured failure envelope will depend on the mode ratio history during the experiment. The symbols in Fig 13 are the RL  $\rho = 0.19 \text{ g/cm}^3$  specimen results now including  $G_{IIc} = 250 \text{ J/m}^2$  (when  $G_I = 0$ ). The experimental results can be explained as a path between initiation toughness ( $95 \text{ J/m}^2$ ) and steady state toughness ( $125 \text{ J/m}^2$ ). The path for a given mixed-mode experiment would depend on the changes in mode I component during the crack propagation. A DCB specimen with crack deviation only allows a small fraction of mode II and therefore these experiments can only give information about a small piece of the mixed-mode failure envelope. We analyzed all other specimens with crack deviations. They all had similar results but corresponded to even smaller portions of the full envelope.

## Conclusions

This paper presents results for crack growth in balsa wood in several directions and under mode I, mode II, or mixed-mode loading. The toughness of balsa is lower than most woods, but closer to other woods they previously expected considering its very low density. In balsa, like other woods, it is important to characterize both initiation and propagation of cracks and find full  $R$  curves. These  $R$  curves show that mode I toughness of balsa is affected by a fiber bridging process zone while mode II toughness is not. This process zone also contributes to unusual mixed-mode failure where  $G_{II}$  can increase along with  $G_I$ .

## Acknowledgements

This work was funded by 3A Composites, Switzerland. We also thank 3A Composites for providing all balsa materials.

## References

- Ashby MF, Easterling KE, Harrysson R, Maiti SK. The fracture toughness of woods. *Proc. Royal Soc. London* 1985; **A398**: 261-280.
- Atack D, May WD, Morris EL, Sproule, RN. The energy of tensile and cleavage fracture of black spruce. *Tappi* 1961; **44**:555–567.
- Atkins AG, Mai YW. Elastic and plastic fracture. New York: John Wiley & Sons; 1985.
- Crouch, BA, Bender RG, Williams JG. An investigation of notching techniques for Fracture-toughness measurement in amorphous nylon, *Engineering Fracture Mechanics* 1992; **41**:49-57.
- Conrad MPC, Smith GD, Fernlund, G. Fracture of discontinuous wood-adhesive bonds. *Int. J. Adhesion & Adhesives* 2003; **23**:39-47.
- DeBaise GR, Porter AW, and Pentoney RE. 1966, Morphology and mechanics of wood fracture. *Mat. Res. Stand.* 1966; **6**:493–499.
- Dreisbach JF. Balsa wood and its properties. Columbia, Connecticut: Colombia Graphs; 1952.
- Easterling KE, Harrysson R, Gibson LJ, and Ashby MF. On the mechanics of balsa and other woods. *Proc. R. Soc. Lond.* 1982; **A383**:31-41.
- Forest Products Laboratory. Wood handbook - Wood as an engineering material. General Technical Report FPL-GTR-190. Madison, WI: U.S. Department of Agriculture, Forest Service, Forest Products Laboratory: 508 p. 2010.
- Gibson LJ, Ashby, MF. Cellular solids: Structure and properties. Cambridge, England: Cambridge University Press; 1997.
- Haygreen JG, Bowyer JL. Forest products and wood science: An introduction. Ames, Iowa, USA: Iowa State University Press; 1995.
- Jeronimidis G. The fracture behaviour of wood and the relations between toughness and morphology. *Proc. Roy. Soc. London* 1980; **B208**:447–460.
- Johnson JA. 1973, Crack initiation in wood plates. *Wood Science* 1973; **6**:151–158.
- Kanninen MF, Popelar CH. Advanced Fracture Mechanics. New York; Oxford University Press; 1985; page 41.
- Martin RH, Davidson B. Mode II fracture toughness evaluation using four point bend, end notched flexure test. *Plastics, Rubber, and Composites* 1999; **28**:401-406.
- Matsumoto N, Nairn JA. The fracture toughness of medium density fiberboard (MDF) including the effects of fiber bridging and crack-plane interference," *Engr. Fract. Mech.* 2009; **76**:2748-2757.
- Matsumoto N, Nairn JA. Fracture toughness of wood and wood composites during crack propagation. *Wood and Fiber Science* 2012; **44**:121-133.
- Nairn JA. Analytical and numerical modeling of R curves for cracks with bridging zones. *Int. J. Fracture* 2009; **155**:167-181.

- Nairn JA. Generalized crack closure analysis for elements with arbitrarily-placed side nodes and consistent nodal forces. *Int. J. Fracture* 2011; **171**:11-22.
- Schniewind AP, Pozniak RA. On the fracture toughness of Douglas fir wood. *Engineering Fracture Mechanics* 1971; **2**:223–233.
- Schniewind AP, and Centeno JC. 1973, Fracture toughness and duration of load factor I. Six principal systems of crack propagation and the duration factor for cracks propagating parallel to grain. *Wood Fiber* 1973; **5**:152–159.
- Strong AB. Fundamentals of composites manufacturing: Materials, methods and applications, second edition, Dearborn, Michigan: Society of Manufacturing Engineers; 2008.
- Sutton MA, Wolters WJ, Peters WH, Rawson WF, McNeil SR. Determination of displacement using an improved digital image correlation method. *Image and Vision Computing* 1983; **1**:133-139.
- Williams JG. Fracture mechanics of polymers. New York: John Wiley & Sons; 1984.
- Williams JG. On the calculation of energy release rates for cracked laminates. *Int. J. Fract.* 1988; **36**:101–119.
- Wilson E., Shir Mohammadi M, Nairn JA. Crack propagation fracture toughness of several wood species. *Advances in Civil Engineering Materials* 2013; in press.

**Table 1.** Finite element analysis (FEA) calculations for the fraction mode I component ( $\varphi = G_I/G$ ) for a DCB specimen with an off-center crack for different values of  $h_2/(h_1+h_2)$  (as defined in Figure 1)

| $h_2/(h_1+h_2)$ | $\varphi = G_I/G$ |
|-----------------|-------------------|
| 0.20            | 0.706786          |
| 0.22            | 0.72407           |
| 0.26            | 0.76489           |
| 0.30            | 0.812206          |
| 0.32            | 0.8374334         |
| 0.36            | 0.889083          |
| 0.40            | 0.937531          |
| 0.42            | 0.958403          |
| 0.48            | 0.997215          |
| 0.50            | 1.00              |

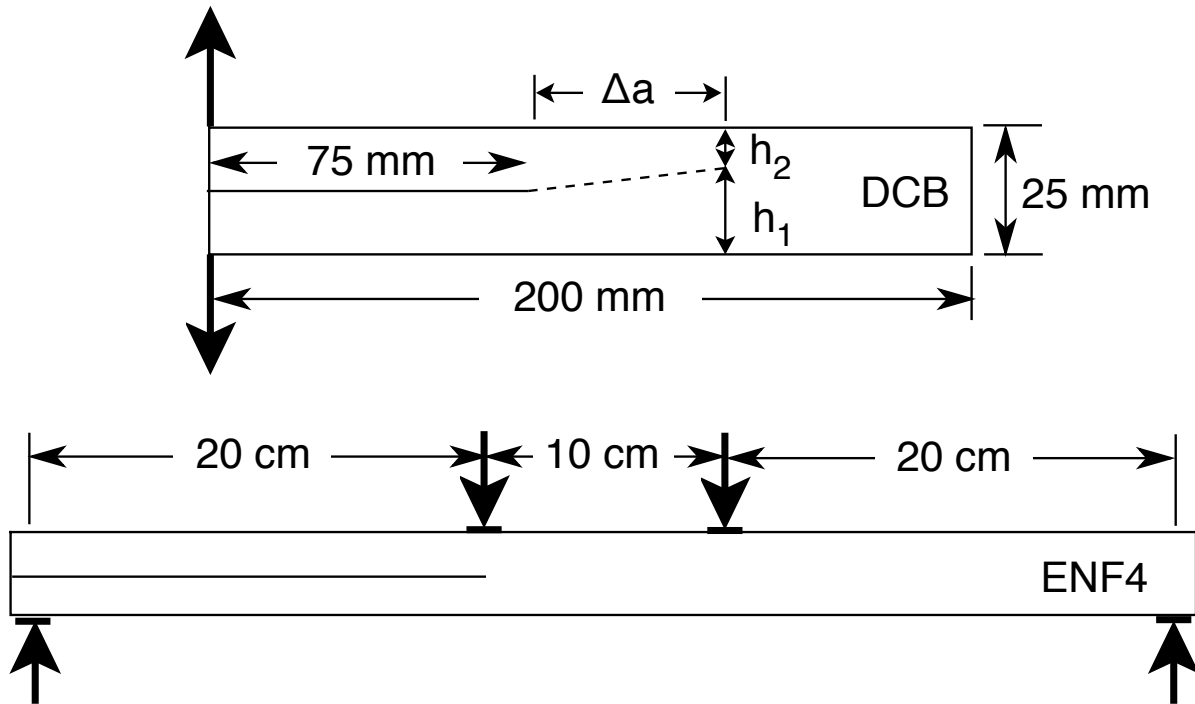


**Figure 1.** The mode I double cantilever beam specimen (DCB) and the mode II, four-point end-notched flexure (ENF4) specimens used for fracture testing. The specimen width is the out of plane dimension. The DCB specimen defines crack growth,  $\Delta a$ , and crack deviation (when it occurred) for dashed crack propagation.

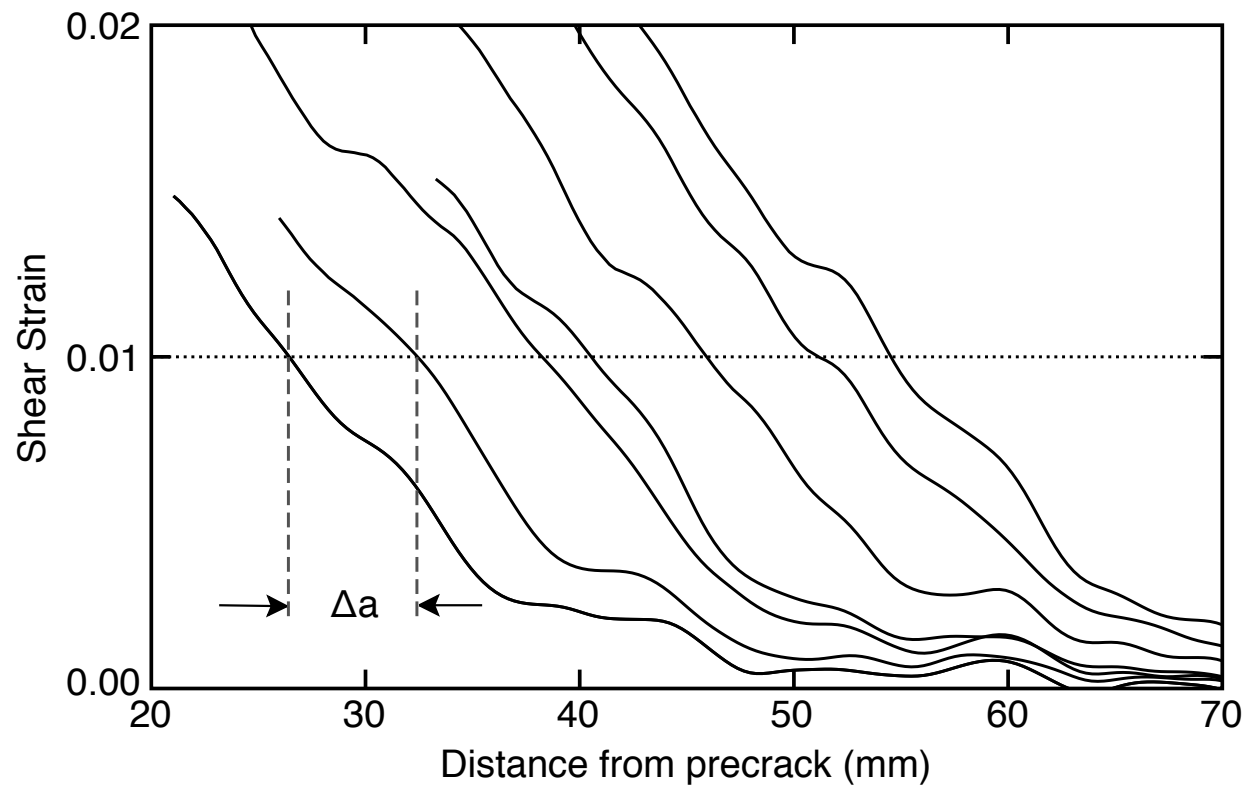


**Figure 2.** The in-plane shear strain as measured by digital image correlation (DIC) ahead of a propagating crack at different times during the experiment. The crack is propagating to the right. The distance between any two curves (*e.g.*,  $\Delta a$ ) is the amount of crack growth that occurred in that time interval.

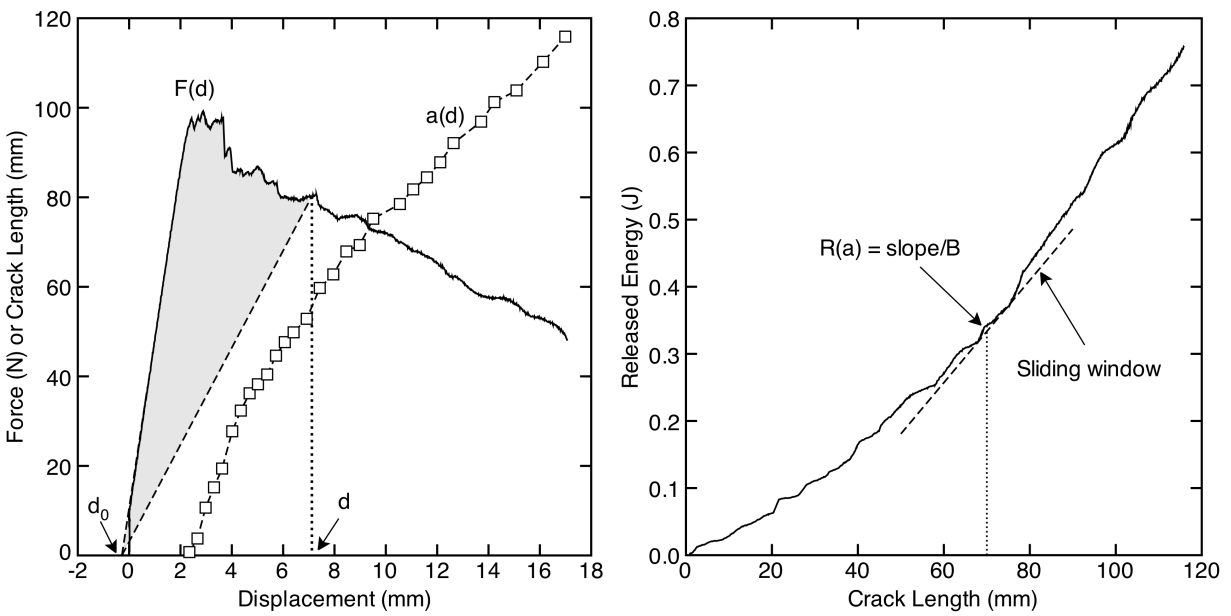


**Figure 3.** An area method for direct calculation of  $R$  curves from synchronized force and crack length data as a function of displacement. The shaded area on the left gives cumulative energy released up to displacement  $d$ . The right side plots this energy as a function of crack length at the same  $d$ . The slope of the curve on the right (per unit thickness) is the  $R$  curve.

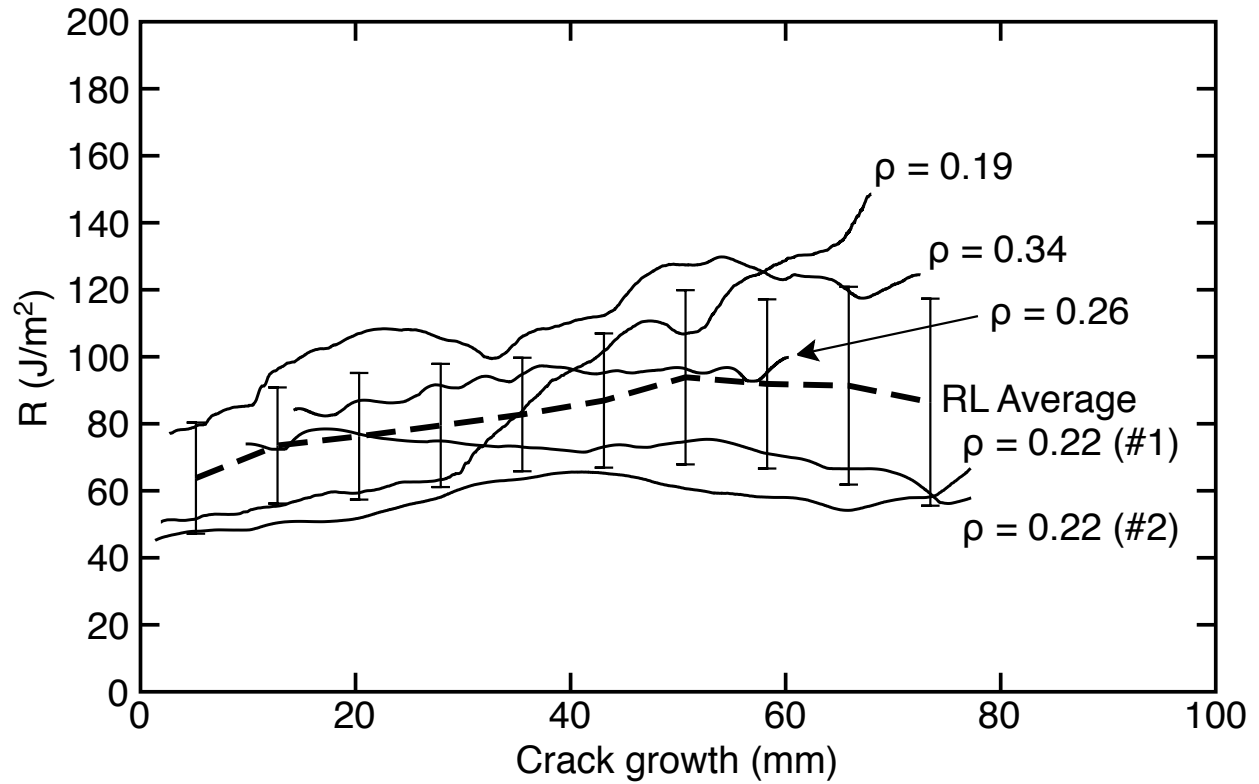


**Figure 4.** *R* curves for five different balsa specimens with mode I crack growth in the RL direction. The densities of the specimens are indicated on the curves. The dashed line is an average (excluding the  $\rho = 0.19$  specimen).

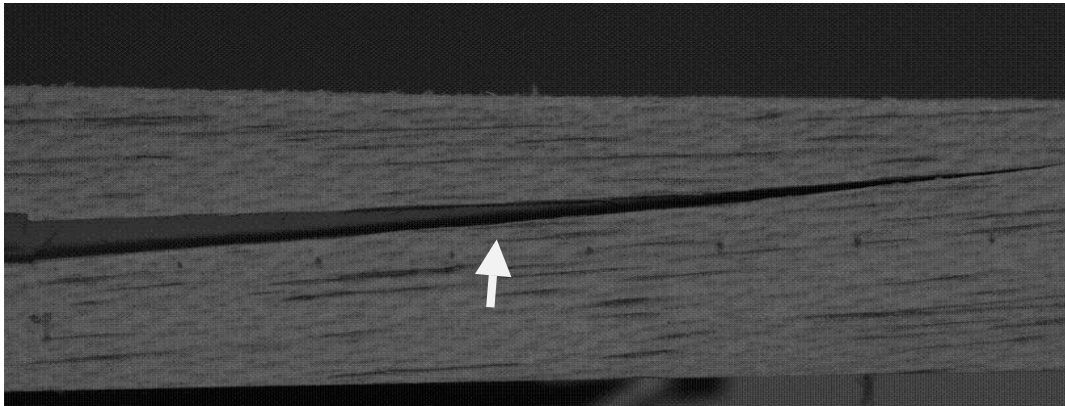


**Figure 5.** The RL balsa specimen with  $\rho = 0.19 \text{ g/cm}^3$  had a crack path that deviated from the midplane of the specimen.

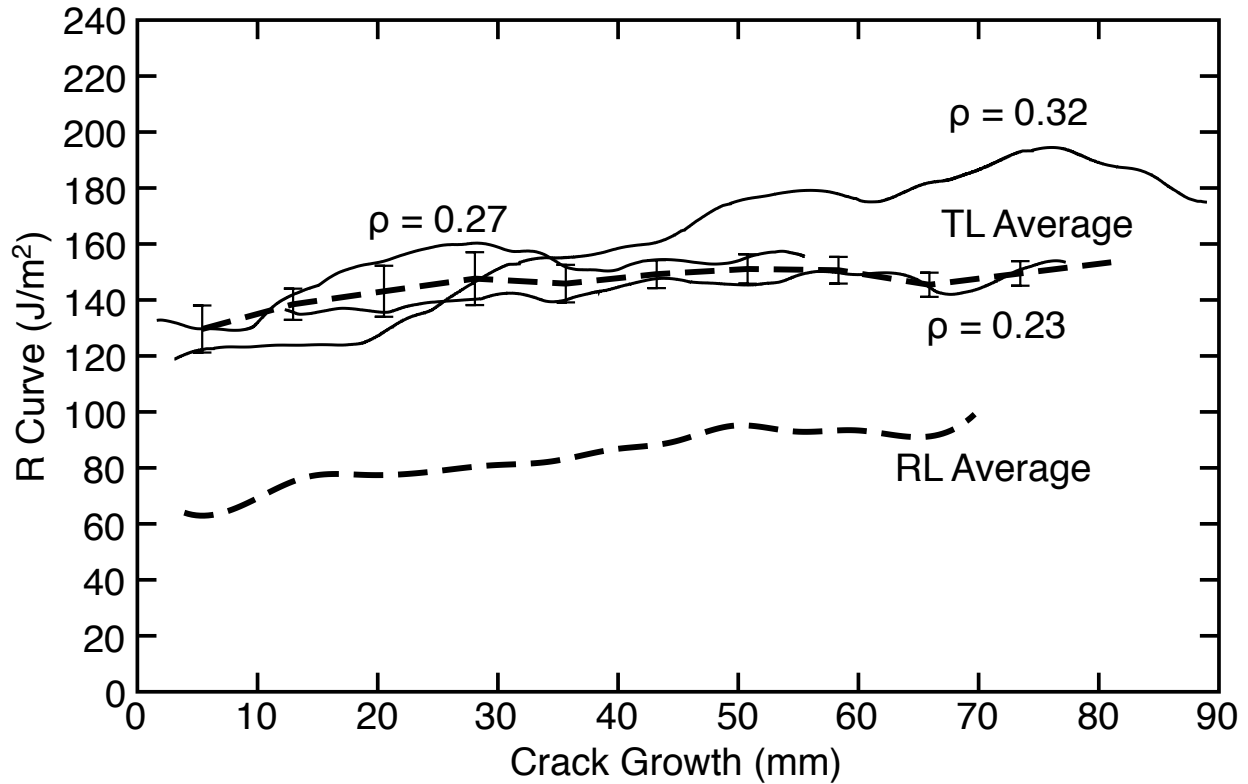


**Figure 6.** *R* curves for three different balsa specimens with mode I crack growth in the TL direction. The densities of the specimens are indicated on the curves. The dashed line is an average (excluding the  $\rho = 0.32$  specimen). The "RL Average" from Figure 4 is included (without error bars) for comparison.

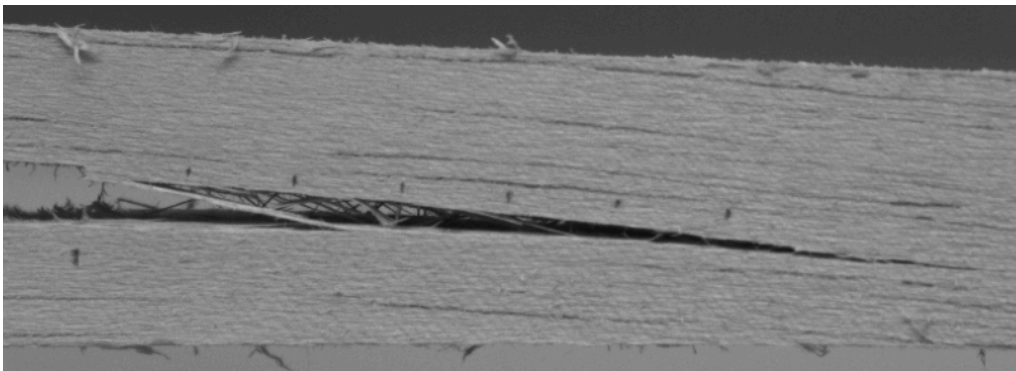


**Figure 7.** The TL balsa specimen with  $\rho = 0.32 \text{ g/cm}^3$  had a crack path that deviated from the midplane of the specimen. The crack plane also shows fibers bridging between the crack surfaces.

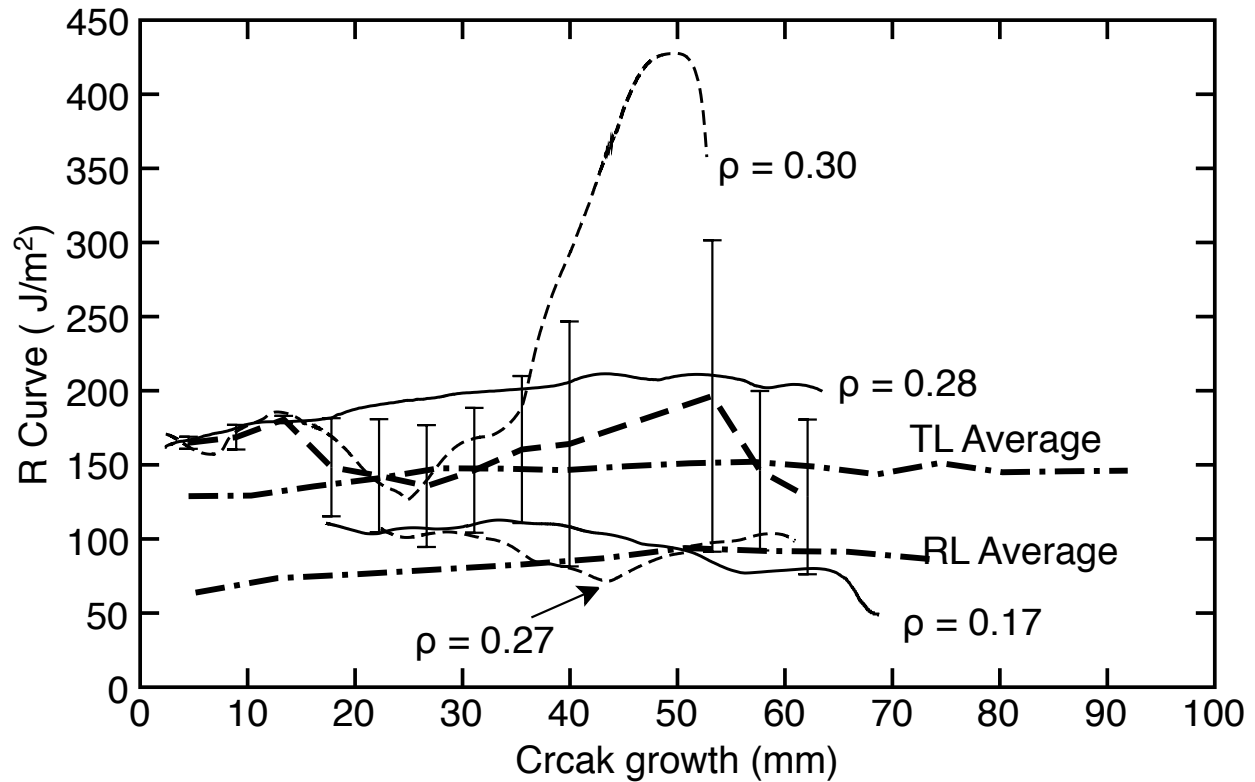


**Figure 8.** *R* curves for four different balsa specimens with mode I crack growth in the RL45 direction. The densities of the specimens are indicated on the curves. The dashed line is an average (excluding the  $\rho = 0.30$  specimen). The "RL Average" from Figure 4 and "TL Average" from Fig 6 are included (without error bars) for comparison.

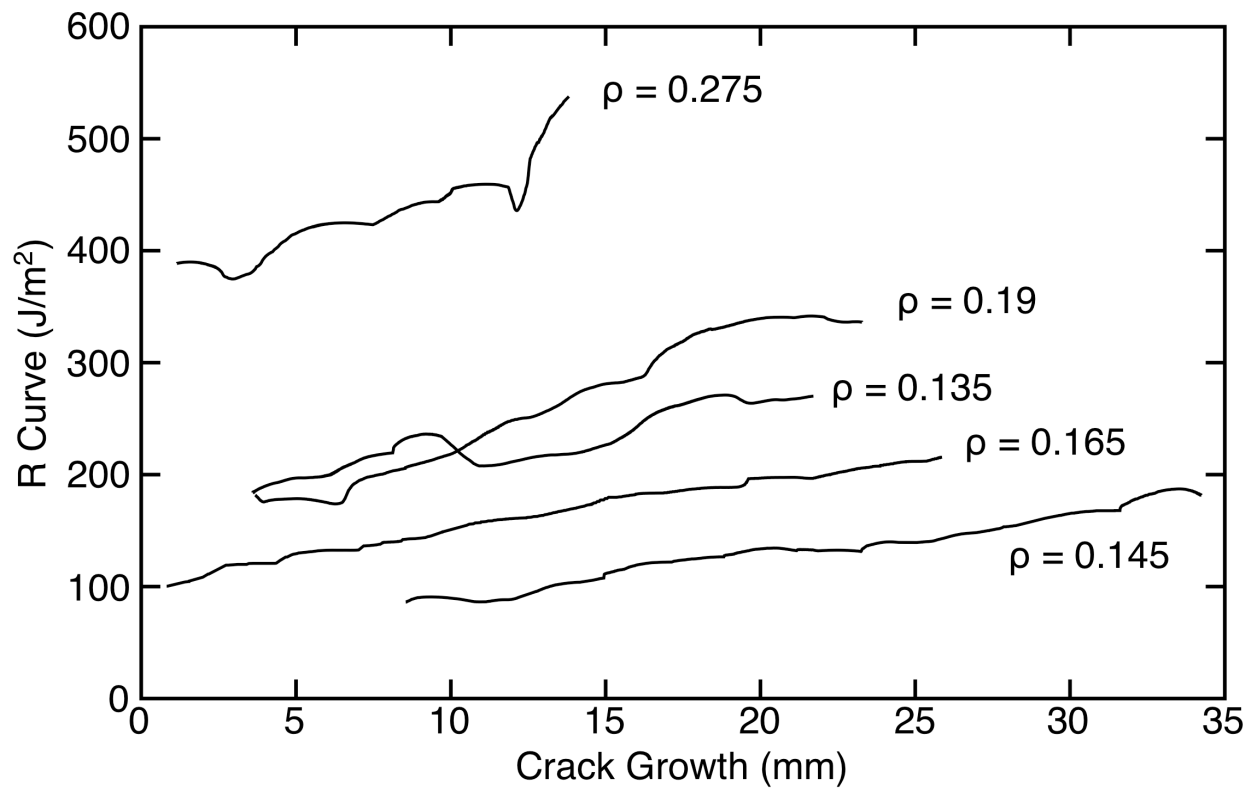


**Figure 9.** *R* curves for five different balsa specimens with mode I crack growth in the RT direction. The densities of the specimens are indicated on the curves.

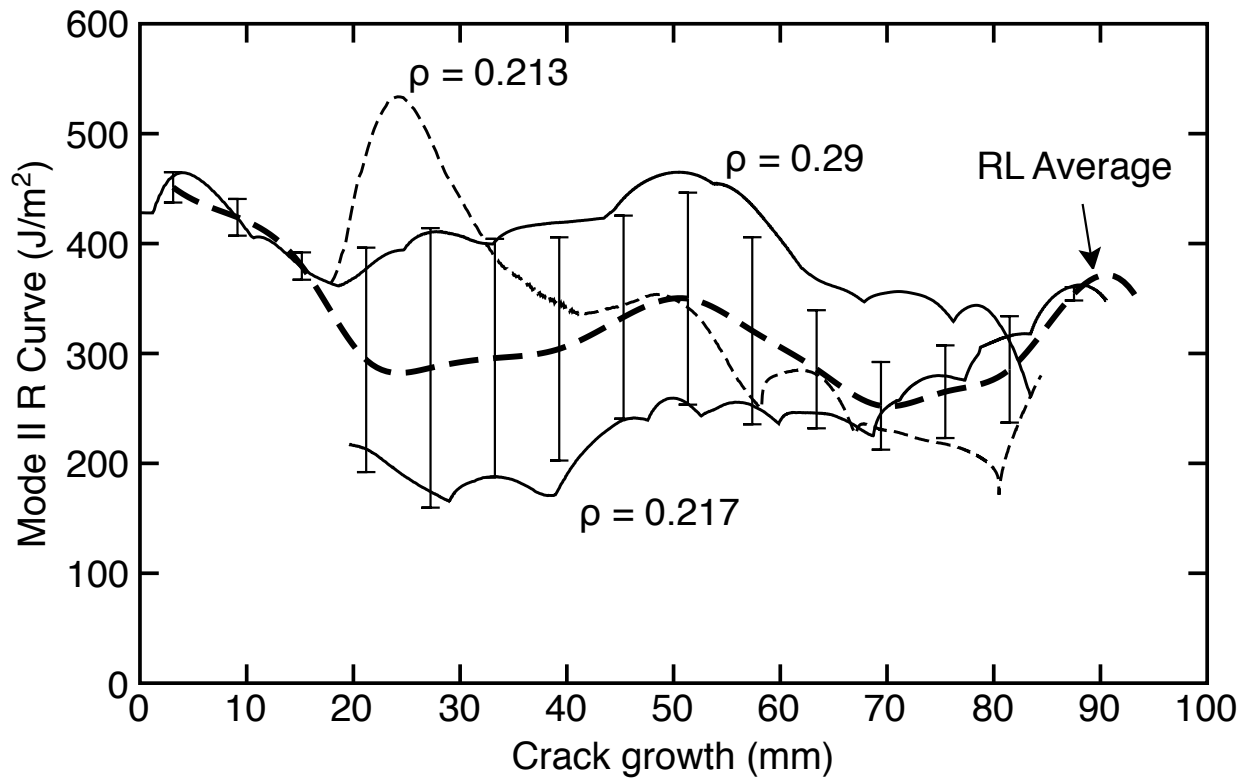


**Figure 10.** *R* curves for three different balsa specimens with mode II crack growth in the RL direction. The densities of the specimens are indicated on the curves. The dashed line is an average.

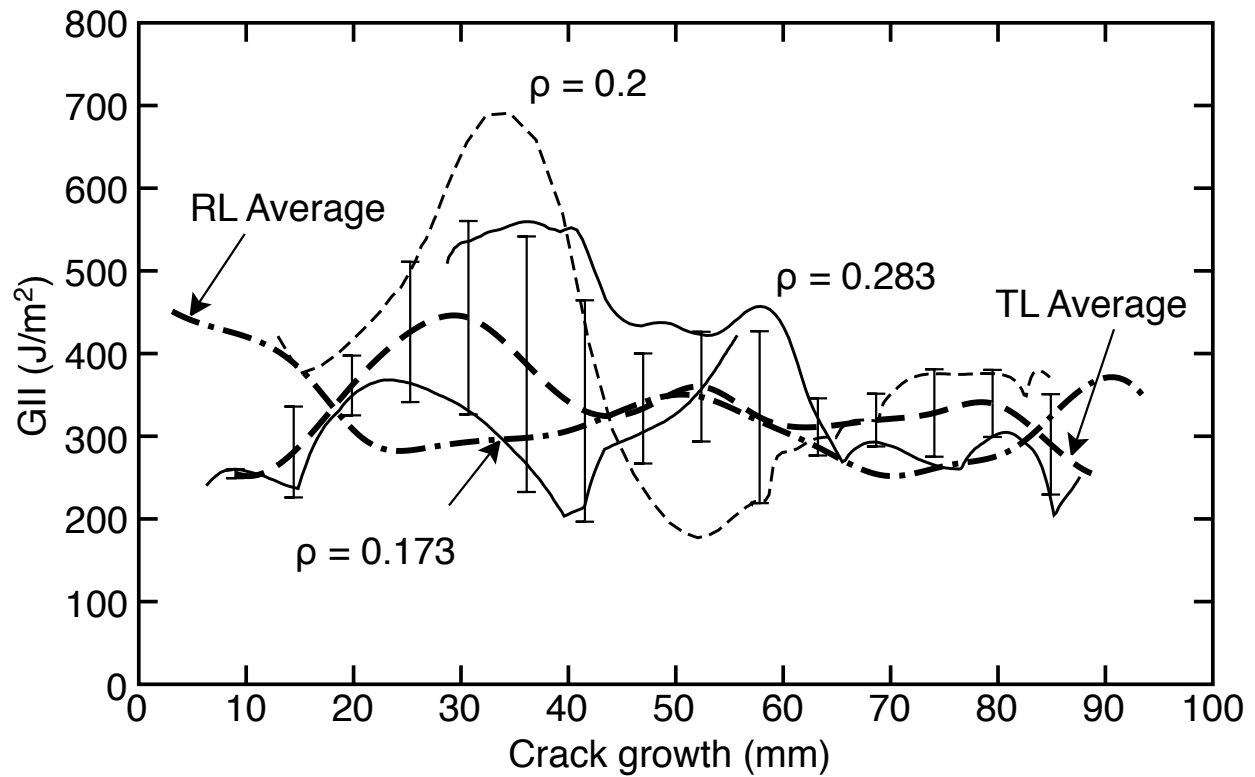


**Figure 11.** *R* curves for three different balsa specimens with mode II crack growth in the TL direction. The densities of the specimens are indicated on the curves. The dashed line is an average. The "RL Average" from Figure 10 is included (without error bars) for comparison.

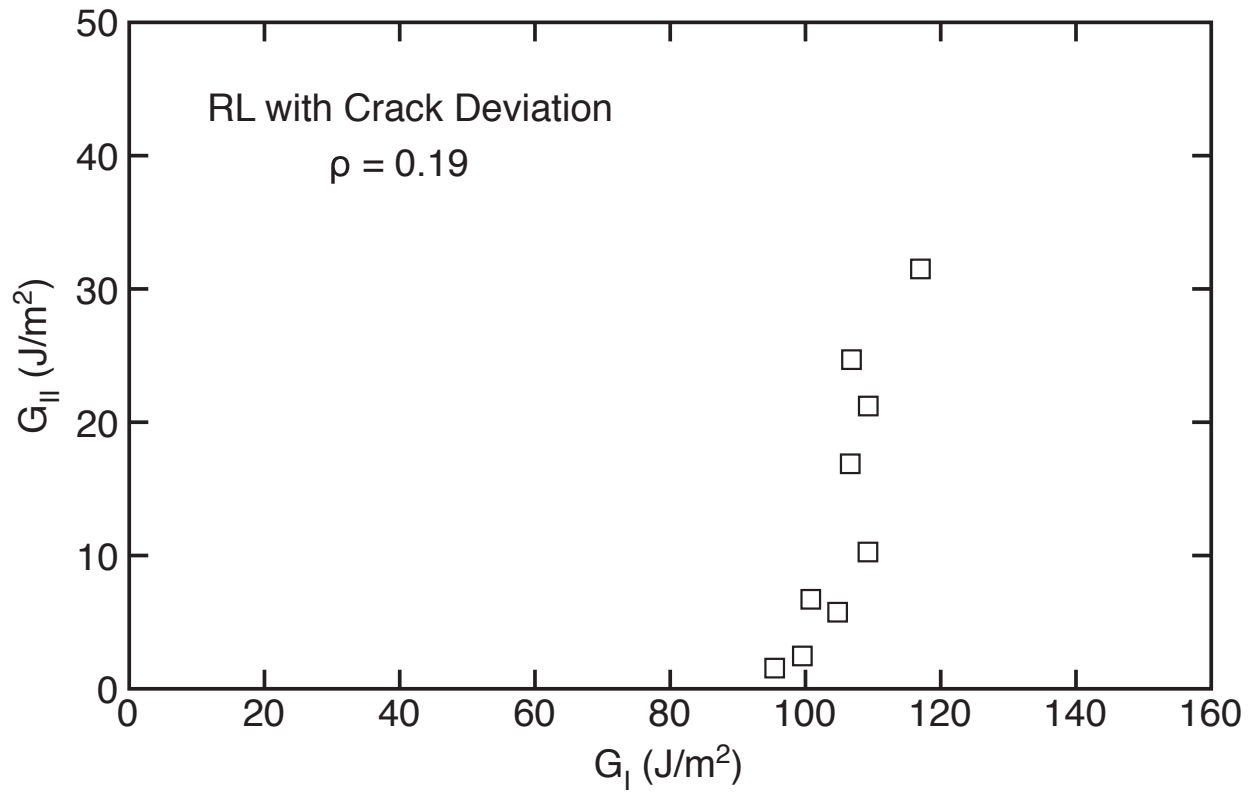


**Figure 12.** A portion for the mixed-mode failure envelope for balsa specimen with  $\rho = 0.19$  g/cm<sup>3</sup> with crack growth in the RL direction. The mixed-mode state was caused by crack deviation from the midplane (see Figure 5).

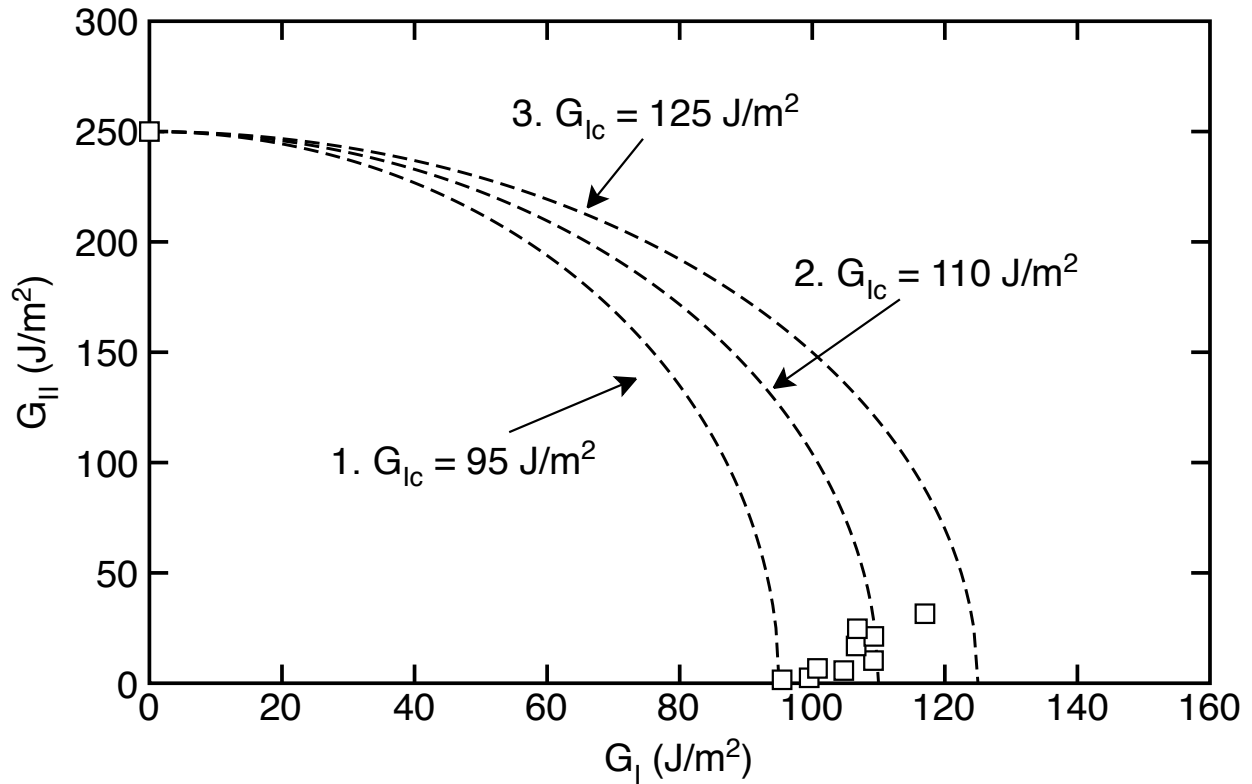


**Figure 13:** Mixed-mode failure envelopes for balsa with crack growth in the RL direction. The dashed lines are hypothetical curves for specimens with constant amounts of fiber bridging. The experimental data correspond to points with variable amounts of fiber bridging and therefore move within these curves.